Defense Technical Information Center Compilation Part Notice

ADP011108

TITLE: Application of Active Core Exhaust Control to Elliminate the Core Thrust Reverser on Heavy Lift Aircraft

DISTRIBUTION: Approved for public release, distribution unlimited

This paper is part of the following report:

TITLE: Active Control Technology for Enhanced Performance Operational Capabilities of Military Aircraft, Land Vehicles and Sea Vehicles [Technologies des systemes a commandes actives pour l'amelioration des performances operationnelles des aeronefs militaires, des vehicules terrestres et des vehicules maritimes]

To order the complete compilation report, use: ADA395700

The component part is provided here to allow users access to individually authored sections of proceedings, annals, symposia, etc. However, the component should be considered within the context of the overall compilation report and not as a stand-alone technical report.

The following component part numbers comprise the compilation report:
ADP011101 thru ADP011178

Application of Active Core Exhaust Control to Eliminate the Core Thrust Reverser on Heavy Lift Aircraft

Clarence F. Chenault*
Air Vehicles Directorate, Air Force Research Laboratory
Wright-Patterson Air Force Base, OH 45433

John D. Dorris[†]
The Boeing Company
2401E Wardlow Road
Mail Code C078-0019
Long Beach, CA 90807-5309

ABSTRACT

Pulsed jet blowing for mixing enhancement in a hot jet is examined using numerical simulation. Numerical simulations have been completed for a sub-scale turbojet engine, a full scale ground demonstration case, and a High-Bypass Ratio Engine (HBRE). These simulations have shown that pulsed jet blowing can significantly reduce jet plume potential core lengths at static and forward flight conditions. The numerical scheme utilizes large timestep implicit integration for efficiency, and a second order physical space algorithm for robustness. The pulsed jet disturbance is calculated directly and a turbulence model is employed to represent the cascade to smaller length scales. Experimental data corresponding to the numerical simulations are also presented and indicate similar benefits from pulsed jet mixing.

INTRODUCTION

Active flow control technology is currently being evaluated for application in many areas of aircraft development. Performance of high-lift systems for transport and combat aircraft could be enhanced by modifying the effective aerodynamic shape of an airfoil or flap. Aircraft designed for minimum radar cross-section may benefit from thrust vectoring by fluidic injection since control surface deflections could be minimized or eliminated. Boundary layer separation in advanced compact inlets and diffusers may be minimized with the application of synthetic or pulsed jets at the appropriate locations. Control of cavity acoustics with pulsed jets has also been demonstrated by Shaw[1].

An application that has shown particular promise for active flow control technology is the enhanced mixing of a jet plume. For the case of large transport aircraft, three benefits may be realized from the active control of the jet plumes. One, the elimination of the need for a core thrust reverser for engine running offload and backing operations, since the core reverser is used primarily for the thermal protection of personnel loading and/or offloading cargo aft of the aircraft. Two, the reduction of flap temperatures while operating in the powered lift portion of the flight envelope. This benefit could lead to the flap surfaces being constructed of lower cost and lighter weight materials. Three, improved flap capture area for better, powered lift field length performance.

The benefits (and limitations) of active control of jet plumes has recently been investigated experimentally in research efforts conducted by the Boeing Company and the USAF. In one case, the centerline plume temperature reduction was measured for a sub-scale, single exhaust, turbojet engine, the J402-CA-700 (nozzle diameter of 6 inches), while under the influence of an opposing pair of pulsed jets near the external nozzle lip. In a second experiment, a full scale JT8D-15 mixed exhaust turbofan engine was modified to bleed air from the compressor to an array of pulsed jets located internally near the nozzle exit. The experimental setup for the JT8D is shown in Figure 1. Concurrent with the JT8D testing, an effort was undertaken to develop a computational methodology for the prediction of plume flowfields incorporating the unsteady pulsed jet technology demonstrated experimentally. This methodology, once validated, could be used to complement the experimental results and further the understanding of this technology. After validation is demonstrated with the results from the J402 and the JT8D simulations, this

---
* ACE Control Program Manager, AIAA Senior Member, email: clarence.chenault@va.afrl.af.mil
† Senior Manager, Advanced Airframe/Aircraft Systems, Boeing Transport and Tanker Technology

methodology is applied to an HBRE configuration with separate exhausts flow paths utilizing take-off mass flow rates.

To simulate flowfields of this nature, large timestep implicit integration is utilized for efficiency. There is no attempt to directly resolve all temporal and spatial scales. The grid resolution and timestep for the calculation is sufficient to resolve the large scale forced disturbance of the pulsed jet. A turbulence model is employed to represent the cascade to smaller scales. Since the turbulence model includes large scale turbulence effects, one should expect this approach to over predict mixing. For each of the nozzle flows, a steady state (unforced) calculation is completed, and then a forced calculation is initiated beginning from the steady state solution.

GOVERNING EQUATIONS

The Boeing (formerly McDonnell Douglas) compressible flow solver, NASTD, developed by Bush[2], is used. NASTD is the precursor to the WIND flow solver available through the NPARC Alliance. The NASTD flow solver incorporates an unsteady arbitrary inflow boundary condition to simulate the pulsed jet flow. In this case, the boundary condition is applied at the location of the pulsed jet nozzle exit, and thus, the flow within the pulsed jet system is not modeled. One, or more, of several fluid properties can be allowed to vary to simulate the pulsed jet. The unsteady fluid property varies in a sinusoidal fashion according to,

$$P(t) = Po + \Delta P \cos(\omega t + \varphi),$$

Where Po denotes the average of the fluid property, ΔP the amplitude of the perturbation, ω the angular frequency, and φ the phase angle.

Grid Generation

The grid generation software, MACGS, developed by Gatzke et al.[3], is used to construct the 3-D computational grids for the J402, JT8D and HBRE simulations. In order to simplify the grid generation process, the geometries of the J402, JT8D and HBRE were assumed to be axi-symmetric. For example, nozzle plug support structure was not included in any of the cases. Thus, all the computational zones are constructed by a simple rotation about the nozzle axis.

For the nozzle cases under consideration, the domain of interest is assumed to be downstream of the nozzle exit. As such, the downstream outflow boundary is placed at least 20 jet diameters downstream of the nozzle exit to prevent any influence of the downstream boundary in the domain of interest. Minimal grid stretching, e.g. 6% to 8%, in the axial direction is employed to properly resolve the primary forced disturbance. The maximum grid spacing is limited to 1/15 of the characteristic wavelength, λ, in the first 10 jet diameters downstream of the jet exit. The characteristic wavelength of the disturbance for the static round jet is given by,

$$\lambda = 0.6 \, ujet / f$$

where ujet is the fluid velocity at the nozzle exit, and f is the pulse frequency in Hertz. The Strouhal number, a dimensionless scaling parameter for this type of calculation, is defined as

$$St = f*Djet/ujet$$

where Djet is the diameter of the nozzle exit.

Timestep

The solution timestep, Δt, is tied to the frequency, f, of the pulsed jets and the stability requirement of the flow solver. It is the stability requirement that sets the maximum allowable timestep for the particular spatial and temporal scheme. The timestep also must resolve the unsteady flow of the pulsed jet, however, with at least 100 timesteps per pulse. Thus,

$$\Delta t = \Delta ymin(CFL)/(ujet+ajet)$$
$$= 1/(\#timesteps/pulse)*f$$

The timestep is adjustable, to a certain extent, through the minimum grid spacing, $\Delta ymin$. The minimum grid spacing, however, is constrained to resolve the smallest features of the nozzle geometry, pulsed jet nozzle exit, and the forced disturbance in the plume.

Turbulence Model

For these calculations, the Menter[4] blended k-ϵ/k-ω shear stress transport (SST) turbulence model is used. For free shear layers, this model is virtually identical to the Jones-Launder[5] k-ϵ model for free shear layers.

RESULTS

An example of the computational grid for the J402 turbojet engine nozzle is shown in Figure 2a. The nozzle exit is at x=6.86 inches. The nozzle walls are embedded in the grid clustering in the lower and upper left of the figure. This clustering becomes the clustering for the nozzle shear layers downstream of the nozzle exit. The nozzle plug and the external annular ring that contains the pulsed jets occupy the space not filled with grid. Topologically, the grid is five zones and 1.144 million grid nodes. The minimum spacing of the grid is 0.0075 inches. Figure 2b shows more grid detail near the nozzle exit and pulsed jet. The minimum grid spacing is in this region near the nozzle exit. The pulsed jet is modeled with an arbitrary inflow boundary condition across four grid points at y=3.15 inches. The pulsed jet width is 0.063 inches located just external to the nozzle exit. Both the upper and lower pulsed jet occupies 90 degrees of circumferential arc.

The computational grid for the full scale JT8D-15 mixed flow turbofan engine nozzle is shown in Figure 3a. The nozzle exit is at x=0.0 inches. The split between the core and fan flow is evident at about y= $\pm$15.0 inches on the far left where the two streams enter the domain. The pulsed jets are located on the internal wall of the nozzle approximately two inches upstream of the nozzle exit. Topologically, the grid is eight zones and 1.48 million grid nodes. The minimum spacing for this grid is 0.025 inches. A close in view of the grid near the pulsed jet and nozzle

exit is shown in Figure 3b. Each of the pulsed jets (upper and lower) has a width of 0.925 inches and occupies 90 degrees of circumferential arc.

The computational grid for the full scale HBRE separate exhaust flow turbofan engine nozzle is shown in Figure 4a. The primary (core) nozzle exit is at x=0.0 inches, with a radius of about 15 inches. The secondary (fan) nozzle exit is upstream of the primary nozzle exit at about x=-80.0 inches, with an outer radius of approximately 40 inches. Topologically, the grid is 13 zones and just over one million grid nodes. The minimum spacing for this grid is 0.10 inches. Unlike the modeling done for the J402 and JT8D, a simplified model of the pulsed jet injector is included for the case of the HBRE. This is done to better simulate the flowfield in the region of the pulsed jet exit and the primary nozzle by removing the pulsed jet boundary condition from the nozzle wall. A close in view of the grid near the pulsed jet and nozzle exit is shown is Figure 4b. The pulsed jet exit is 1.5 inches upstream of the primary nozzle exit. Each of the pulsed jets (upper and lower) has a width of 0.80 inches and occupies 45 degrees of circumferential arc. An axial cut through the grid at x=-1.5 is shown in Figure 4c. The physical domain of the pulsed jet injector zones (upper and lower) indeed overlaps the primary nozzle external zone. This overlap, however, is visual only. Computationally, these zones are disconnected.

Pulsed Jet Model

There is more than one way to specify the pulsed jet flow for these calculations. NASTD/WIND allows for time varying Mach.number, pressure (total or static), temperature (total or static), angle of attack, angle of yaw, or velocity, at an arbitrary inflow boundary. The user may even specify a combination of any, or all, of these flow variables. From the experimental results, details of the pulsed jet flow, e.g. Mach number variation at the pulsed jet exit, were not available. The total mass flow of the pulsed jet system, however, was known. Assuming a constant static pressure at the pulsed jet exit, an average Mach number (and temperature) of the pulsed jet is deduced. The variation in Mach number, however, is subjective. For both the J402 and the JT8D configuration, the pulsed jets consisted of an opposing pair covering 90 degrees of circumferential arc for each jet, pulsed harmonically, 180 degrees out of phase.

For the case of the J402, the fluctuation of the pulsed jet exit Mach number from the average Mach number was ±38% (Mach=0.66±0.25). A plot of the pulsed jet mass flow over one cycle is shown in Figure 5a. The total mass flow for the pulsed jet system is 0.21 lbm/sec, or approximately 3% of the primary nozzle flow.

For the JT8D, the fluctuation of the pulsed jet exit Mach number from the average Mach number was ±72% (Mach=0.58±0.42). For this case, a plot of the pulsed jet mass flow over one cycle is shown in Figure 5b. The total mass flow for the pulsed jet system is 6.53 lbm/sec, again approximately 3% of the primary nozzle flow.

For the HBRE, the boundary condition for the pulsed jet is applied differently than the previous cases since the actual pulsed jet is being modeled. A harmonically varying total pressure is applied at the inflow of the pulsed jet model. Thus, the Mach number variation at the pulsed jet exit is dependent on the supply total pressure. For this case, the variation was on the order of 0.1 at minimum mass flow and 0.5 at maximum mass flow. A plot of the pulsed jet mass flow over one cycle is shown in Figure 5c. The total mass flow for the pulsed jet system is 2.84 lbm/sec, or approximately 1.5% of the primary nozzle flow.

J402 Simulation Results (Single Exhaust)

Qualitative comparisons of the effects of pulsed jet mixing for the J402 are shown in Figure 6. The contours are of static temperature. Figure 6a shows an unforced or steady state simulation of the plume. A snapshot in time of the forced simulation is shown in Figure 6b. In this view, the cut is through the plume centerline and the circumferential midpoint of the pulsed jets and depicts the flapping mode of the simulation. In this configuration, the amplitude of the flapping plume is well in excess of the nozzle exit diameter. Time averaged static temperature contours are shown in Figure 7. Figure 7a shows the flapping plane, which is essentially the time average of the flapping depicted in Figure 6b. Figure 7b is a view of the transverse plane, or the plane perpendicular to the flapping plane, and does not cut through either of the opposing pulsed jets.

Quantitative comparisons of the time averaged static and total temperature along the plume centerline for the computational and experimental results are shown in Figure 8. Beginning at two nozzle diameters downstream, the computational results predict a dramatic temperature reduction along the plume centerline. At five nozzle diameters downstream, a temperature reduction of 600 degrees is predicted. The experimental results show a similar trend. Discrepancies between the computational and experimental results are expected due to the simplification of the geometry and flow conditions of the computational model, particularly those of the pulsed jet.

JT8D Simulation Results (Mixed Exhaust)

Quantitative comparisons of the time averaged static and total temperature along the JT8D plume centerline for the computational and experimental results of are shown in Figure 9. As in the case of the J402, beginning at roughly two nozzle diameters downstream, the computational results predicted a dramatic temperature reduction along the plume centerline. At six nozzle diameters downstream, a reduction in total temperature of 550 degrees is predicted. The experimental results for this case are shown at 10 nozzle diameters downstream of the nozzle exit.

Notice for this case a marked increase in the static and total temperature of the primary nozzle flow at the nozzle exit. The increase in the total temperature is caused by bleeding the primary engine flow as a source for the pulsed jet flow. The bleeding of the engine also results in a 4% reduction in total pressure of the core flow. The combination of these two effects increases the static temperature on the plume centerline at the nozzle exit roughly 100 degrees F. This effect can be seen in the first two nozzle diameters downstream of the nozzle exit.

Similar qualitative comparisons for the JT8D are shown in Figure 10. As before, contours of static temperature are shown. Figure 10a shows the unforced or steady state simulation. Figure 10b depicts a snapshot of the forced simulation in the flapping plane, the plane that contains a cut through the pulsed jets. As was the case in the J402 simulation the amplitude of the flapping plume exceeds the nozzle exit diameter. Figure 10c is the time averaged static contour levels for the plume in the flapping plane.

HBRE Simulation Results (Separate Exhausts)

The HBRE simulation is the only one of the calculations done for a forward flight condition. Specifically, a takeoff condition at sea level with a freestream Mach number of 0.24. The primary flow NPR is 1.52 with a total temperature of 1014 F. The secondary flow NPR is 1.72 with a total temperature of 157 F. Once again, qualitative comparisons similar to the J402 and JT8D simulations are shown in Figure 11. As before, contours of static temperature are shown. Figure 11a shows the unforced or steady state simulation predictions. Figure 11b depicts a snapshot of the forced simulation in the flapping plane, the plane that contains a cut through the pulsed jets, and Figures 11c and 11d are the time averaged static contour levels for the plume in the flapping plane and transverse plane, respectively.

Quantitative comparisons of the time averaged static and total temperature along the HBRE configuration's centerline are shown in Figure 12. The diffusion of the core exhaust plume of the HBRE configuration is significantly slower than that observed for the cases of the J402 and JT8D. This is due to the influence of the secondary flow that envelops the core flow. One effect of the secondary flow is to increase the convection velocity of the disturbance responsible for mixing, thus increasing the distance downstream of the core nozzle exit where significant temperature reduction along the plume centerline is evident.

An additional effect of the secondary flow is depicted in Figure 11d. The mixing of the plume is naturally most effective in the geometric plane that contains the pulsed jets, the flapping plane. In the plane perpendicular to the flapping plane, the transverse plane, the plume has a natural tendency to bifurcate. For the J402 and JT8D, with no secondary flow, the bifurcation is minimal. For the HBRE, the secondary flow exasperates the bifurcation. Future work will focus on optimizing the pulsed jet configuration, particularly for the HBRE.

CONCLUSIONS

An efficient computational methodology has been developed for the analysis of unsteady pulsed jet mixing flowfields. The benefits of pulsed jet mixing at sea level static conditions are evident in the reduction of plume centerline temperatures aft of approximately two to three nozzle diameters downstream of the nozzle exit. Furthermore, significant differences in plume expansion characteristics are observed between single and mixed exhaust configurations and separate exhaust configurations.

ACKNOWLEDGEMENTS

REFERENCES

1   Shaw, L., 1998, "Active Control of Cavity Acoustics," Proc 4th AIAA/CEAS Aeroacoustics Conference, June 2-4, Toulouse, France.
2   Bush, R.H., 1988, "A Three Dimensional Zonal Navier-Stokes Code for Subsonic Through Hypersonic Propulsion Flowfields," AIAA Paper 88-2830.
3   Gatzke, T.G., LaBozzetta, W.F., Finfrock, G.P., Johnson, J.A., and Romer, W.W., 1991, "MACGS: A Zonal Grid Generation System for Complex Aero-Propulsion Configurations," AIAA Paper 91-2156.
4   Menter, F.R., 1991, "Zonal Two Equation k-ε Turbulence Models for Aerodynamic Flows," AIAA 93-2906.
5   Jones, W.P., and Launder, B.E., 1973, "The Calculation of Low-Reynolds-Number Phenomena with a Two-Equation Model of Turbulence," International *Journal of Heat and Mass Transfer*, 16, pp.1119-1130.
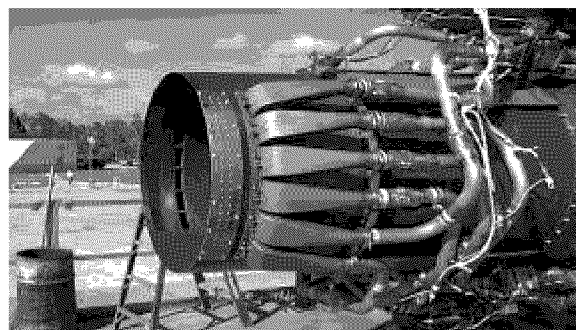

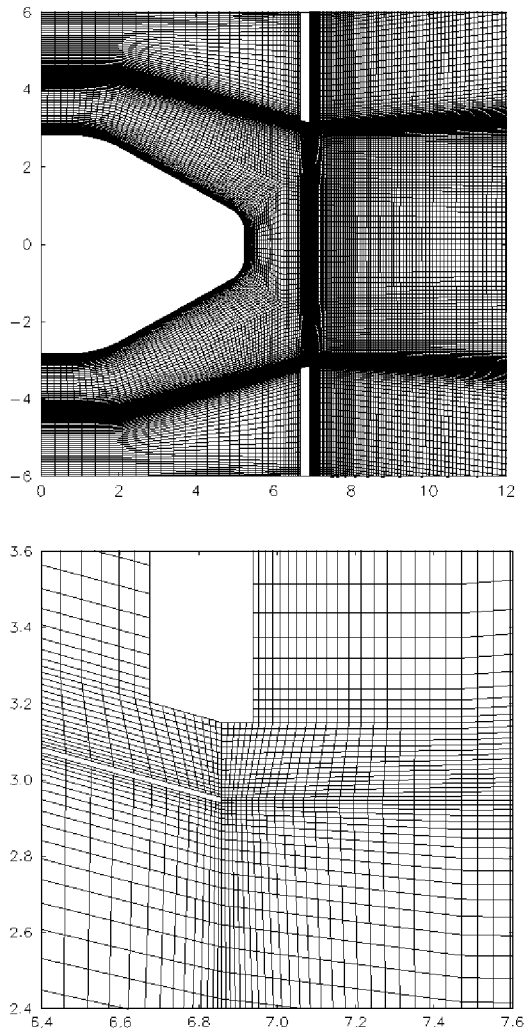Figure 1. JT8D full scale engine pulsed jet experimental setup

Figure 2. J402 computational grid in the region of the a) nozzle exit, b) nozzle lip and externally pulsed jet.
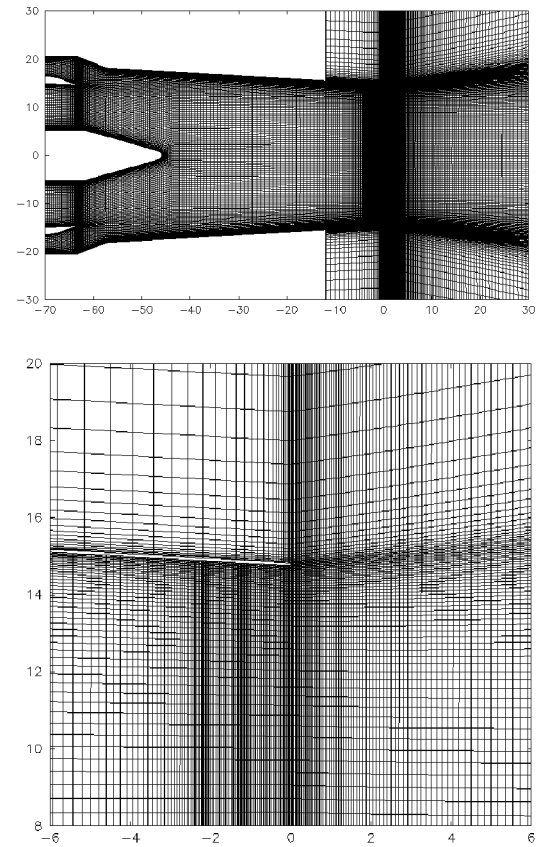
Figure 3. JT8D computational grid in the region of the a) nozzle exit, b) nozzle lip and externally pulsed jet.
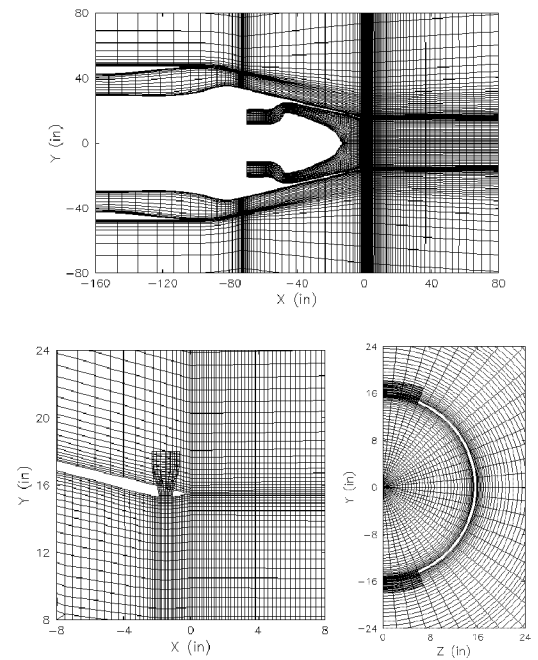
Figure 4. HBRE computational grid in the region of the a) nozzle exit, b) nozzle lip, c) external pulsed jet.
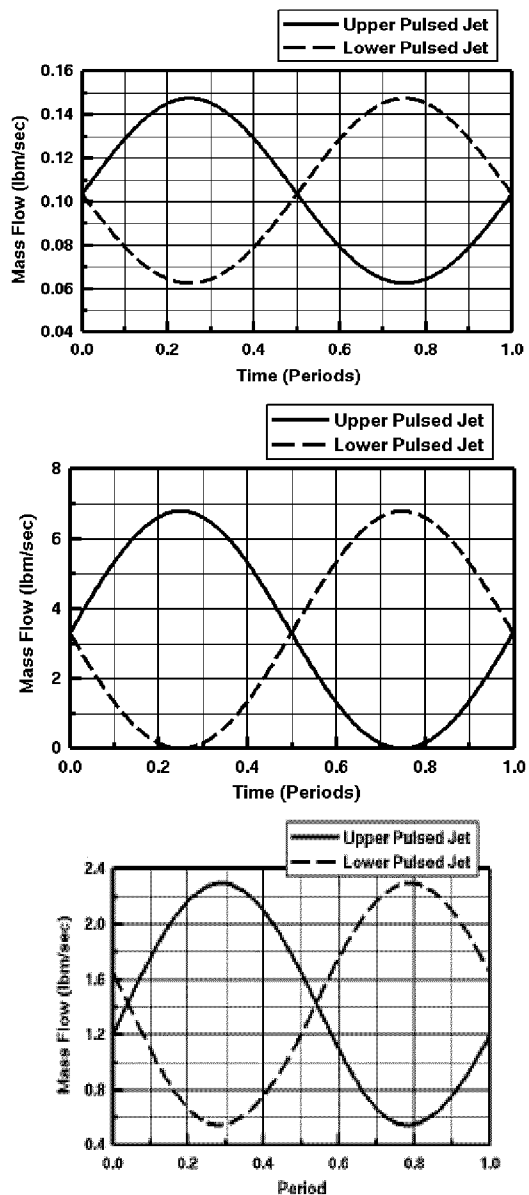
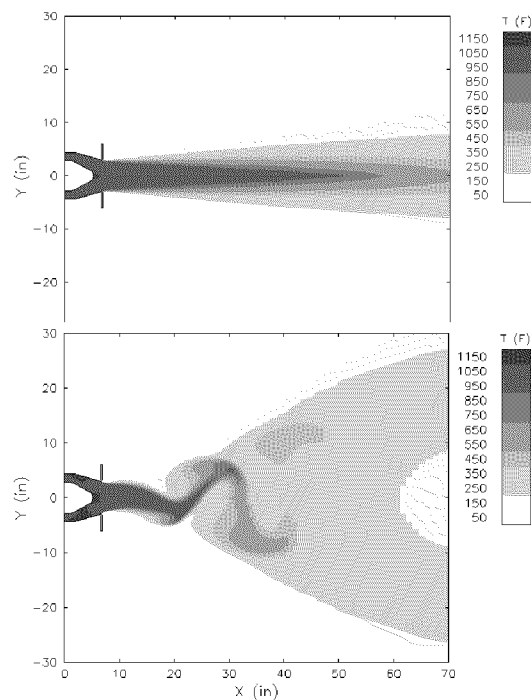Figure 5. Mass flow for the pulsed jet systems over one cycle a) J402, b) JT8D, c) HBRE.

Figure 6. Static temperature (°F) contours from the J402 simulation a) unforced (steady state), b) snapshot of the flapping plane at maximum mass flow of the lower pulsed jet.

Figure 7. Time average static temperature contours from the J402 forced simulation a) flapping plane, b) transverse plane.
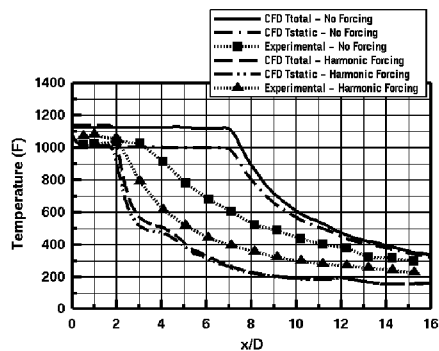
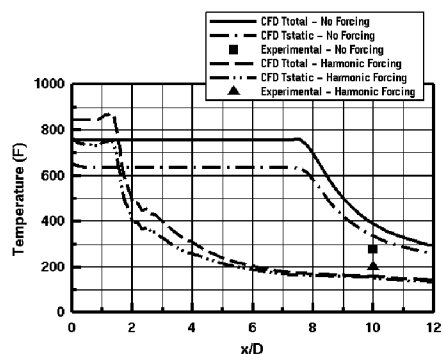Figure 8. Time averaged plume centerline temperatures for the J402

Figure 9. Time averaged plume centerline temperatures for the JT8D
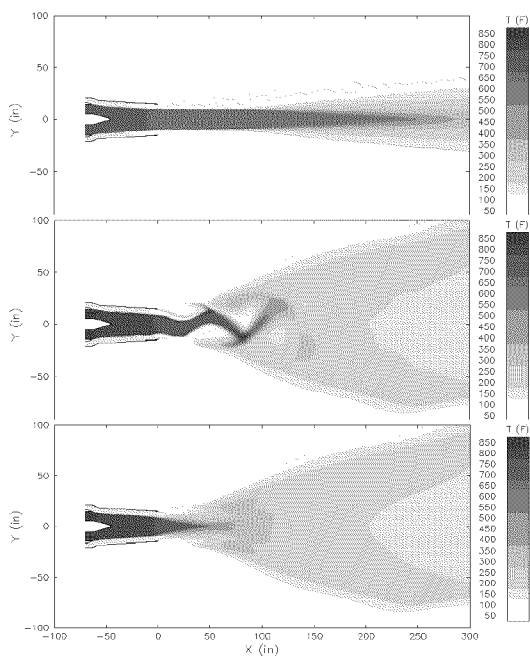

Figure 11. Static temperature (F) contours from the HBRE simulations a) unforced (steady state), b) snapshot of the forced simulation in the flapping plane, c) time average of the forced simulation in the flapping plane, d) time average of the forced simulation in the transverse plane

Figure 12. Time averaged plume centerline temperatures for the HBRE

Figure 10. Static temperature (F) contours from the JT8D Simulations a) unforced (steady state), b) snapshot of the forced simulation in the flapping plane at maximum mass flow of the upper pulsed jet, c) time average of the forced simulation in the flapping plane
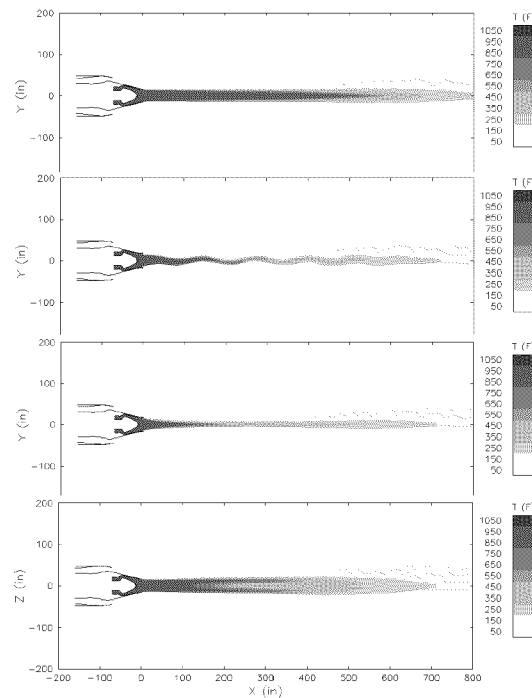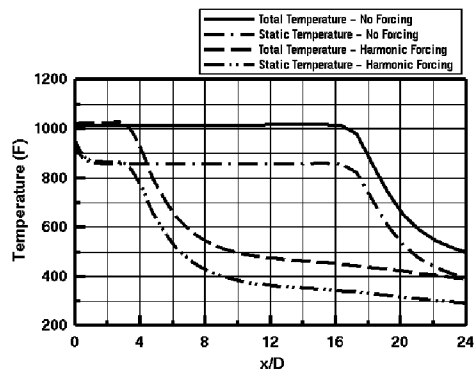
Paper #10

Q by David J Moorhouse: Your first conclusion says an efficient computational methodology was developed, but it overpredicts the measured temperature reduction. You pointed out what was not modeled. It seems like an important result to show what improvements are needed for future CFD development. Please comment.

A. (C. F. Chenault): A comparison of the temperature predictions for the forced and unforced cases clearly implies that turbulence modeling in the root cause of the overprediction. Turbulence is introduced by many mechanisms in the acted turbine engine. Some of these are turbine swirl, steps and gapes in the nozzle surface and from the combustion process. None of the processes or surface imperfections are modeled. These items were ignored because we were only looking for gross flow characteristics and not exact quantities. The large error in the unforced solution was considered acceptable since we were not interested in the region with the large error.

If this is an area where one wishes to improve the prediction. I would recommend modeling the turbine swirl and introduce an initial level of turbulence. If this fails, then a turbulence model tailored for free jet shear flows should be used outside of the nozzle

Q by G.E.A. Meier: Did the periodic control for mixing increase also increase the noise level?

A. (C.F. Chenault): Yes, noise levels did increase on the JT8D Test by 5db →20db depending on the power setting, pulse frequency and the mass flow rate.